



كلية الهندسة - جامعة بغداد



اعضاء اتحاد الجامعات العربية

Thermal performance study of Air Jet Impingement on a Flat Plate with Copper Foam

Dhafar Fadhil Ali¹ and Sajida Lafta Ghashim^{2,*}

¹ Department of Mechanical Engineering, University of Baghdad, Baghdad, Iraq, Dhafar.fadhel@gmail.com

² Department of Mechanical Engineering, University of Baghdad, Baghdad, Iraq, sajda_lafta@yahoo.com

*Corresponding author: Dhafar Fadhil Ali, email: Dhafar.fadhel@gmail.com

Published online: 31 March 2025

Abstract— An experimental investigation of the thermal performance of a single rectangular slot jet impinging on a copper foam flat plate was carried out. The copper foam was 10 mm thick, and 90% porosity was used. Experiments have been performed at various Reynolds numbers from 5200 to 14000 and at different slot-to-plate distances from 2 to 8. Results showed the most enhancement of local Nusselt number appeared at copper foam flat plate compared to smooth flat plate. The effect of pore density on the local and average Nusselt number of a copper foam flat plate with pore densities of 10 PPI and 40 PPI was studied. The local and average Nusselt number of a copper foam flat plate with a pore density of 10 PPI exhibits a higher augmentation than that of a copper foam flat plate with a pore density of 40 PPI. The effect of slot-to-plate distance on local and average Nusselt numbers is studied. In the case of the smooth flat plate, the local Nusselt number slightly rises as slot-to-plate distance increases. In the case of the copper foam flat plate, the flow equally permeates the heat sink when the slot-to-plate distance increases. Flow deflection is more substantial for metal foams with little slot-to-plate distance and a low pore density. However, the augmentation in Reynolds number allows the flow to penetrate the porous medium more evenly.

Keywords— Jet impingement, A pore density of the copper foam, Unconfined slot jet, Local Nusselt number, Copper foam.

1. Introduction

Jet impingement cooling offers enormous heat transfer. As a result, it works well for cooling electronic components, drying textile goods, and cooling turbine blades. Many academics have studied jet impingement by taking a flat plate into account Issac et al. [5], Nirmalkumar et al. [12], and Vinze et al. [16].

Joshi and Sahu [6] investigated the influence of elliptical and circular nozzles of identical equivalent diameters impinging over flat and curved surfaces. They studied Reynolds numbers ranging from 11,250 to 22,500, jet-to-surface spacing of 1 to 6, and different aspect ratios of nozzles 1 to 4. They compared the thermal behavior of concave and flat surfaces. They found that with an increase in the aspect ratio of the nozzle from 1 to 4, the largest improvement in the stagnation Nusselt number was identified on both flat and curved surfaces. Diop et al. [18] investigated the enhancement of the heat transfer coefficient of the target surface under jet impingement

employing suitable velocity and sufficient impact distances to guarantee effective cooling. According to the experimental data, the jet-to-surface distances of 4, 7, and 9 at a velocity of 15 m/s had the maximum rate of heat transfer when compared to other values. Dhruw et al. [10] experimentally studied the heat transfer characteristics between a target surface and a circular jet impingement. They studied jet-to-surface distances of 3–20 d, with Reynolds numbers ranging from 10,000 to 45,000 for the region range of $0 \leq r/d \leq 44$. They showed that an accurate understanding of the jet's cooling phenomenon at any point over the plate may be obtained from the combined heat transfer analysis of both local and area averages. It was observed that the Nusselt number increases at various locations as the mass flow rate increases.

Conventional heat sinks are no longer suitable for going to waste the generated heat necessitating the development of creative solutions to the expanding thermal management issues. Due to the significant heat transfer potential from combining two cooling technologies, heat transfer by jet

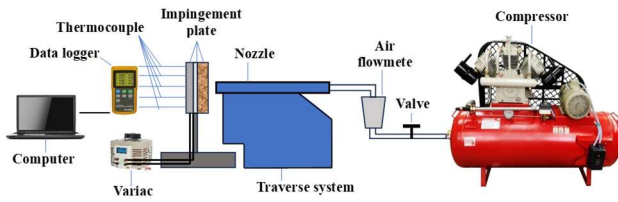


Figure 1: Schematic representation of the experimental test

Impingement and open-cell metal foams has recently drawn attention. The porous media were used in many researches by Hussain and Saleh [4], Karamallah et al. [1], Amori and Khalaf [8], Ali [11], Mohammed [2], and Ali and Ghashim [15].

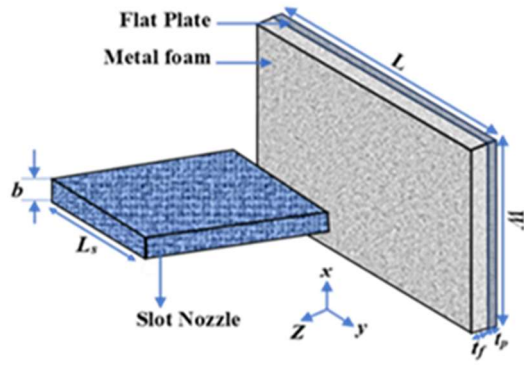
Yakkatelli et al. [17] studied the porosity of foam, jet-to-plate distance, and Reynolds number using visualization of smoke-wire flow. They found that the jet-to-surface distance had a major impact on the flow dynamics. With a reduced jet-to-surface distance, the flow is significantly deflected due to the ligature structure's impact velocity. An increased nozzle-to-surface distance leads to a lower impact velocity at the foam's upper surface, allowing more flow to enter the heat sink more evenly. Additionally, it was shown that the flow enters the porous material more evenly when the laminar to turbulent jet's Reynolds number is increased, which decreases the recirculation region at the foam exit. Shih et al. [19] examined the metal foam heat sinks' restricted flow outlets under jet-impinging flow circumstances. By controlling the height of the metal foam sink's flow outlet, an annular mask of restricting flow forces cooling air to reach the generation heat surface. They used the flow restricting masks to enhance the heat transfer of heat sinks. Singh et al. [13] experimentally investigated the heat transfer characteristics of a copper foam flat plate under a circular jet impingement. They used a thickness of copper foam of 4 mm and 6 mm at a porosity of 90 % and a density of pore 10 PPI. They studied different nozzle-to-plate distances at Reynolds number 23000. The results showed that thermal performance had increased in the wall jet zone of the plate with thin metal foam than in a plate with thick metal foam. Yogi et al. [9] studied the characteristics of heat transfer of an impinging jet on an aluminum foam flat plate. Experiments were performed on Reynolds numbers ranging from 5200 to 12,000 and slot-to-plate spacing ($z/b = 2-10$). Aluminum foam has a porosity of 92%, a thickness of 8mm, and a density of pores of 10, 20, and 40 PPI. They observed that the Nusselt number of an aluminum foam flat plate with a pore density of 10 PPI is higher than that of an aluminum foam flat plate with a pore density of 20 PPI and 40 PPI.

The study aims to experimentally examine the local and average Nusselt number under jet-impinging conditions on a copper foam flat plate. The investigation studied pore density, slot-to-plate distance, and Reynolds number. The primary goal was to determine the pore density of copper foam that achieves the highest heat transfer rates.

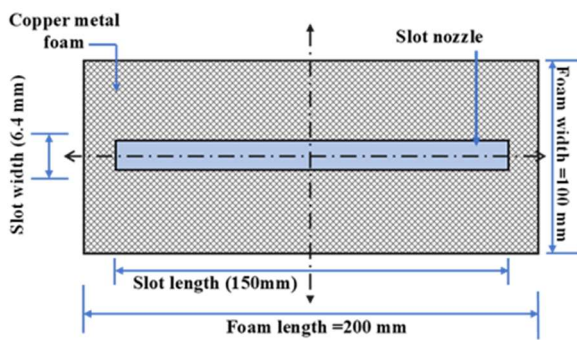
2. Experimental Investigation

2.1 Experimental setup

The schematic diagram of the present experimental setup is shown in **Figure (1)**. Airflow was received from a compressor. A gate valve was fitted downstream of the compressor to control the airflow rate and provide the desired Reynolds number. The nozzle was fed a constant air flow rate using a Glass Tube Rotameter air flowmeter ranging from 0–120 m³/hour. A polyurethane tube with a 12 mm diameter and 2 mm thickness between the compressor and flow meter and the flow meter and nozzle was used as a connection. A nozzle is a rectangular slot of 150 mm length (L_s) and 6.4 mm width (b), and it was created through a 3D printer. The aspect ratio of the nozzle cross-section (about 24) was maintained as reported by [12]. A fully developed flow requires an upstream length 25 times larger than the hydraulic diameter at the nozzle's exit as reported by [12, 9]. The assembly of the target plate is shown in **Figure (2)**. The dimensions of 200 mm × 100 mm and a 3 mm thick aluminum plate served as the impinging target heated surface. A resistive cartridge heater measuring 10 mm in diameter and 200 mm in length was mounted inside an aluminum plate to create a hot plate (heat source). At maximum load, this heater produces almost 300 W of heat. The heater receives AC from the voltage regulator. Clamp meters with a range and accuracy of 0 to 2000 ± 0.5% A are used to measure currents. A ceramic fiber board (10 mm thick) is affixed to the face bottom of the heated plate to reduce heat losses. Five Chrome-Alumel (K-type) thermocouples are positioned on the backside of the base flat plate (opposite to the impinging nozzle) at 20 mm pitch starting from the stagnation point towards the ends (with a stream wise direction) to measure the temperature of the target plate. As a result, the local wall temperature measured on the front or impingement side is regarded as equal to that recorded on the rear surface. Three thermocouples are positioned (with span wise direction) used to measure heater temperature and three to measure the temperature of the air jet at the outlet of the nozzle. The thermocouples underwent calibration before being installed. The temperature is measured using a digital thermometer (12 channels with memory card; model: BTM-4208SD, Lutron Company, Taiwan). A calibrated hot wire anemometer (Yk-2005AH model, serial number Q634196, Lutron Company) was positioned immediately after the jet exit and in the middle of the nozzle to monitor the airflow velocity. The transverse system is used to set the impinging surface. It is ensured that the impingement surface is perpendicular to the jet axis and is approximately geometrically centered with a jet axis. The tests were conducted for slot-to-plate distances (z/b) of 2, 4, 6, and 8. **Figure (3)** shows that the entire nozzle body and the target surface are kept over a table and oriented according to a guide so they can be easily moved for different slot-to-plate distances. **Figure (4)** illustrates the two types of copper foam (10 and 40 PPI) employed in this investigation. Copper foam is applied to the aluminum flat plate using a thermal paste.



a) 3-D view



b) The view of the cross-section and dimensions in mm

Figure 2: The test section view

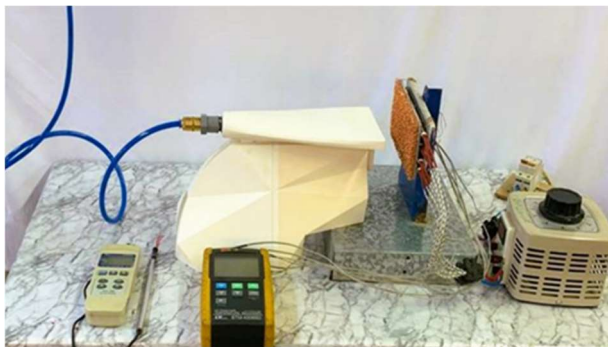
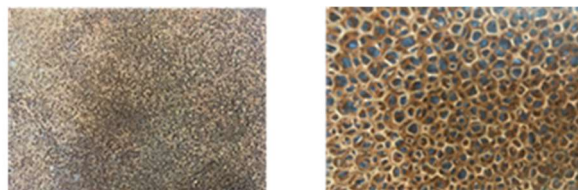


Figure 3: Plate of the test section of the experimental setup



a) 40 PPI

b) 10 PPI

Figure 4: Photograph of the types of copper foam that are used in the present study

2.2 Data Reduction

A slot jet Reynolds number is determined by

$$Re = \frac{\rho vb}{\mu} = \frac{\dot{m}}{\mu L_s} \quad (1)$$

At the jet exit temperature T_j , all air qualities are assessed. The target surface temperature is calculated by taking the average of five spots on the surface that thermocouples recorded during the experiment. Applying electric heat flux causes the aluminum plate to generate volumetric heat. The jet fluid will convert the heat applied to the plate, and radiation and natural convection will cause some heat to escape into the surrounding air. As a result, the energy balance over the plate is represented as

$$q_{loss} = q_{rad} + q_{nat} \quad (2)$$

$$q_{joule} = \frac{VI}{A} \quad (3)$$

$$q_{conv} = q_{joule} - q_{loss} \quad (4)$$

q_{loss} Is heat loss from the hot plate which is neglected in this work.

The forced convective heat transfer coefficient may be found using

$$h = \frac{q_{conv}}{(T_w - T_j)} \quad (5)$$

Nusselt number is obtained by

$$Nu = \frac{hb}{k_{air}} \quad (6)$$

$$\overline{Nu} = \frac{\overline{h}b}{k_{air}} \quad (7)$$

2.3 Uncertainty Analysis

Analyzing uncertainty for temperature, mass, time, and length were all measured directly [15]. The gadget manufacturers made faults that led to uncertainty in these data. There were inaccuracies of \pm in the voltage, current, width, and length of ± 0.01 V, 0.01 A, 0.0005 m, and 0.0005m, respectively. The temperature reading error of the thermocouple was $\pm (0.05)^\circ\text{C}$. Utilizing uncertainty analysis, Reynolds and Nusselt numbers were determined. The estimation of uncertainty related to systematic error and random error was assessed [7] recommended methodology. The source of the uncertainty is:

$$\delta R = \frac{\partial R}{\partial x_1} \delta x_1 + \frac{\partial R}{\partial x_2} \delta x_2 + \dots + \frac{\partial R}{\partial x_n} \delta x_n \quad (8)$$

$$W_R = \left[\left(\frac{\partial R}{\partial x_1} W_1 \right)^2 + \left(\frac{\partial R}{\partial x_2} W_2 \right)^2 + \dots + \left(\frac{\partial R}{\partial x_n} W_n \right)^2 \right]^{\frac{1}{2}} \quad (9)$$

As an illustration

The local Nusselt number depends on the number of parameters, which are all susceptible to uncertainty:

$$Nu = F(V_o, I, b, A_s, \Delta T_{w,x})$$

$$\text{Where; } \Delta T_{w,x} = T_w - T_{j,x}$$

The uncertainty can be given as follows;

$$W_{Nu} = \left[\left(\frac{\partial Nu_x}{\partial V_o} \cdot W_{V_o} \right)^2 + \left(\frac{\partial Nu_x}{\partial I} \cdot W_I \right)^2 + \left(\frac{\partial Nu_x}{\partial b} \cdot W_b \right)^2 + \left(\frac{\partial Nu_x}{\partial A_s} \cdot W_{A_s} \right)^2 + \left(\frac{\partial Nu_x}{\partial \Delta T_x} \cdot W_{\Delta T_x} \right)^2 \right]^{\frac{1}{2}} \quad (10)$$

Or,

$$\frac{W_{Nu}}{Nu} = \left[\left(\frac{W_{V_o}}{V_o} \right)^2 + \left(\frac{W_I}{I} \right)^2 + \left(\frac{W_b}{b} \right)^2 + \left(\frac{W_{A_s}}{A_s} \right)^2 + \left(\frac{W_{\Delta T_x}}{\Delta T_x} \right)^2 \right]^{\frac{1}{2}} \quad (11)$$

The Reynolds and Nusselt numbers have respective uncertainties of 13% and 3.98%.

3. Numerical Investigation

Numerical simulation was used to evaluate the temperature distribution on the impingement surface and estimate heat transfer coefficients. The finite-element program ANSYS Fluent 2021R1 was used to run the simulation. **Figure (5)** displays the study's solution domain and boundary conditions. The boundary conditions are the entrainment zone (the pressure outlet) and the nozzle exit (the velocity inlet). Better mesh quality was achieved using a 3D structured grid to mesh the solution domain. In the three-dimensional model, spacing 1 gave 8400000 elements and 8853139 nodes. The cell type was a hexahedral cell model. After reaching a successful mesh, the models were exported to fluent for setup and analysis processes. The RANS-based standard $k-\epsilon$ equation model provides strong and acceptable accuracy for the chosen solution domain as the model for the turbulence. The trials used a 50 W power supply from an AC power source, and the average value was determined by measuring the temperature using thermocouples once a steady state was reached. Likewise, the cartridge heater's volumetric heat generation was assumed during the simulations. Temperatures were determined by obtaining the area-weighted average on the surface of a flat plate. It is found that there is an agreement between the average temperatures on the impinging surface determined by numerical simulations and experiments.

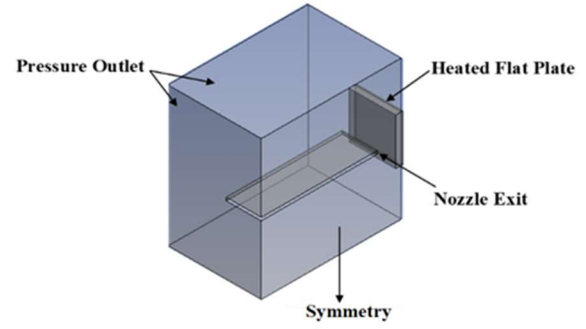


Figure 5: Domain of numerical simulation with boundary conditions

The Navier-Stoke equations (RANS), which are stated as follows, need to be solved in the numerical simulations of [4]:

$$\frac{\partial(\rho u_i)}{\partial x_i} = 0 \quad (12)$$

$$\rho u_j \frac{\partial u_i}{\partial x_j} = -\frac{\partial p}{\partial x_i} + \frac{\partial}{\partial x_j} \left[\mu \left(\frac{\partial u_i}{\partial x_j} + \frac{\partial u_j}{\partial x_i} \right) - \overline{\rho u'_i u'_j} \right] \quad (13)$$

$$\rho u_j \frac{\partial T}{\partial x_j} = \frac{\partial}{\partial x_j} \left[\frac{\mu}{Pr} \frac{\partial T}{\partial x_j} - \overline{\rho T' u'_j} \right] \quad (14)$$

The terms $-\overline{\rho u'_i u'_j}$ and $\overline{\rho T' u'_j}$ in the Eq. (13) and Eq. (14) represent the Reynolds stress term and specific turbulent heat flux respectively.

The $k-\epsilon$ turbulence model has reported more accurate findings for heat transfer by jet impingement with less computing work. It included two transport equations: one for the turbulent kinetic energy (k) and another for the turbulent dissipation rate (ϵ) [14];

$$\frac{\partial}{\partial x_i} (\rho u_i k) = \frac{\partial}{\partial x_i} \left(\frac{\mu_t}{\sigma_k} \frac{\partial k}{\partial x_i} \right) + \mu_t \left(\frac{\partial u_i}{\partial x_j} + \frac{\partial u_j}{\partial x_i} \right) \frac{\partial u_i}{\partial x_j} - \rho \epsilon \quad (15)$$

$$\frac{\partial}{\partial x_i} (\rho u_i \epsilon) = \frac{\partial}{\partial x_i} \left(\frac{\mu_t}{\sigma_\epsilon} \frac{\partial \epsilon}{\partial x_i} \right) + C_{1\epsilon} \frac{\epsilon}{k} \mu_t \left(\frac{\partial u_i}{\partial x_j} + \frac{\partial u_j}{\partial x_i} \right) \frac{\partial u_i}{\partial x_j} - C_{2\epsilon} \rho \frac{\epsilon^2}{k} \quad (16)$$

The turbulent eddy viscosity is then related to k and ϵ by the expression $\mu_t = C_\mu \rho \frac{k^2}{\epsilon}$. The

coefficients $C_\mu, C_{1\epsilon}, C_{2\epsilon}, \sigma_k, \sigma_\epsilon$ are constants that have the following empirically derived values; $C_\mu = 0.09, C_{1\epsilon} = 1.44, C_{2\epsilon} = 1.92, \sigma_k = 1.0, \sigma_\epsilon = 1.3$

The governing equations of metal foam include [15]:

Continuity equation

$$\frac{\partial(\rho u_i)}{\partial x_i} = 0 \quad (17)$$

Momentum equation

$$\frac{\partial(\rho u_i u_j)}{\partial x_i} = -\beta \frac{\partial p}{\partial x_i} + \frac{\partial}{\partial x_j} \left((\mu + \mu_t) \left(\frac{\partial u_i}{\partial x_j} + \frac{\partial u_j}{\partial x_i} \right) \right) - \beta \left(\frac{\mu}{\alpha} u_i + \frac{\rho C_F}{\sqrt{\alpha}} |u| u_i \right) \quad (18)$$

The energy equation for the model of local thermal equilibrium:

$$\beta \frac{\partial(\rho C_p u_j T)}{\partial x_j} = k_{eff} \frac{\partial}{\partial x_j} \left(\frac{\partial T}{\partial x_j} \right) \quad (19)$$

4. Results and Discussion

Measurements of the Nusselt number on a copper foam flat plate impinging an unconfined slot air jet are made through experiments. Foams made of copper metal with a thickness of 10 mm and pore densities of 10 and 40 PPI at 90% porosity are utilized. The slot-to-plate distance ($z/b = 2, 4, 6, \text{ and } 8$) and Reynolds number ($Re = 5200, 9600, \text{ and } 14,000$) are the parameters that are studied.

4.1 Verification of the experimental methodology

The results obtained from experimental data are validated with CFD simulations data to determine the heat transfer characteristics and the behavior of jet impingement on a copper foam flat plate with a pore density of 10 PPI at $z/b = 2$ and $Re = 5200$. **Figure (6)** compares the local Nusselt number of the target plate for the computational and experimental results. The graphic illustrates how well the numerical data match the experimental data. **Figure (7)** displays the average Nusselt number deviation for various slot-to-plate distances. The maximum difference between the experimental and numerical results of the local and average Nusselt numbers are 3.12% and 4.17%, respectively.

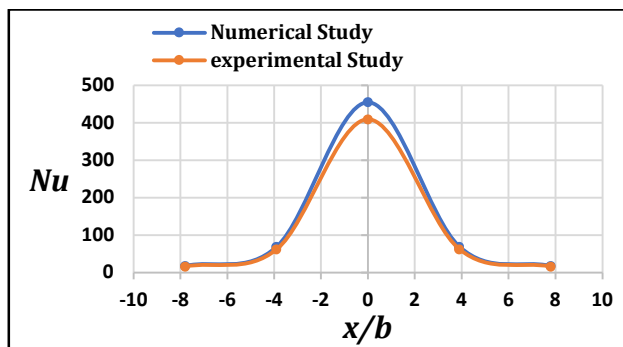


Figure 6: Comparison between the experimental and numerical results of the local Nusselt number distribution (copper foam flat plate of the density of pore of 10 PPI at $z/b=2$ and $Re=5200$).

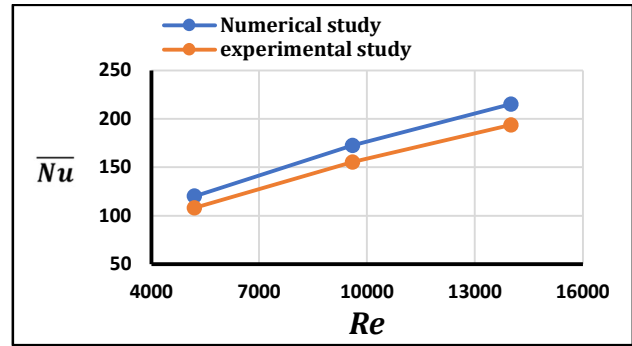
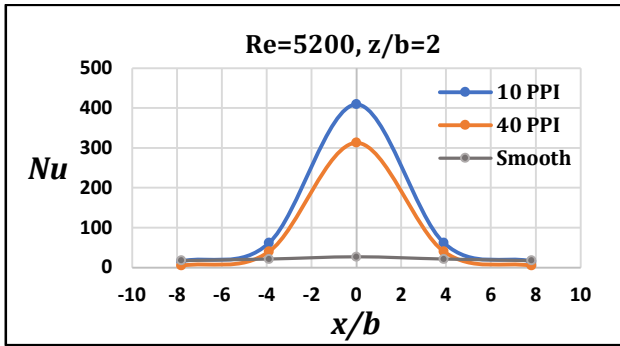


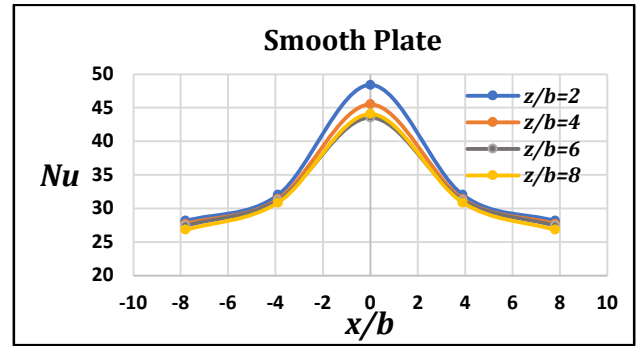
Figure 7: Comparison between the experimental and numerical results of the average Nusselt numbers of copper foam flat plate of the density of pore of 10 PPI with different Reynolds numbers and slot-to-plate distance of 2.

4.2 The local Nusselt number (Nu)

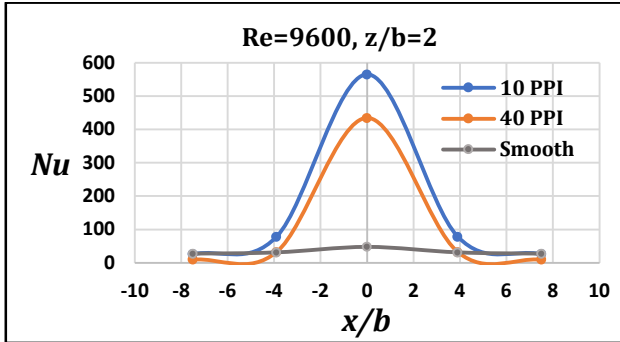
The effects of increasing the Reynolds number on the local Nusselt number of a jet impinging on a smooth flat plate and a copper foam flat plate with a pore density of 10 and 40 PPI at a distance of $z/b = 2$ are depicted in Figures (8a–c). Results illustrated that the local Nusselt number enhancement was higher at a copper foam flat plate than at a smooth flat plate. Similar observations are reported by [8] and [9]. In the stagnation point, the local Nusselt number of a copper foam flat plate was higher compared to the smooth flat plate irrespective of the pore density. Because a small amount of the air jet that cannot pass through the metal foam is bypassed from the top surface of the metal foam when an air jet impinges on the top of the metal foamed flat plate (due to direct impingement on the metal foam ligaments at the top surface of the foam). After passing through the metal foam, the remaining jet fluid strikes the intended surface. The metal foam's porous nature causes the entering jet fluid to split into several micro jets [3]. Compared to a smooth flat plate, the stagnation Nusselt number of the copper foam flat plate may increase due to this array of micro-jets at the stagnation zone. The local Nusselt number is highest in the stagnation region and decreases in the stream wise direction. In experiments, the local Nusselt number grows as the Reynolds number increases. Because the jet's growing momentum as the Reynolds number rises leads to an enhancement in forced convection heat transfer, the flow greatly influences the convective heat transfer of the target plate. An increasing amount of heat transfer on the target plate is provided by flow. Jets are, however, more widely dispersed with the flow if the flow rate is increased excessively. Therefore, convective heat transfer is increased by the jet impingement. In most cases, the peak local Nusselt number was attained at a pore density of 10 PPI. In contrast, the pore density of 40 PPI produced the lowest local Nusselt values. It was shown that when the density of pores decreased, the local Nusselt number of a copper foam flat plate increased.



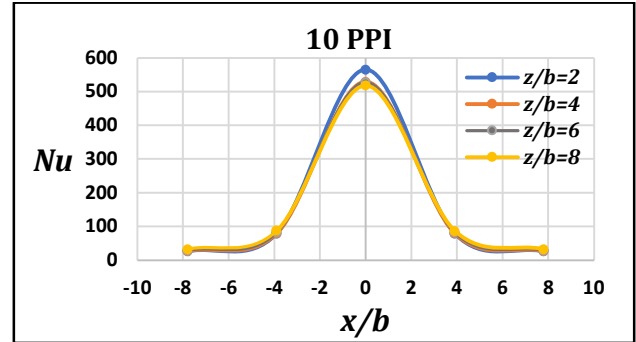
(a)



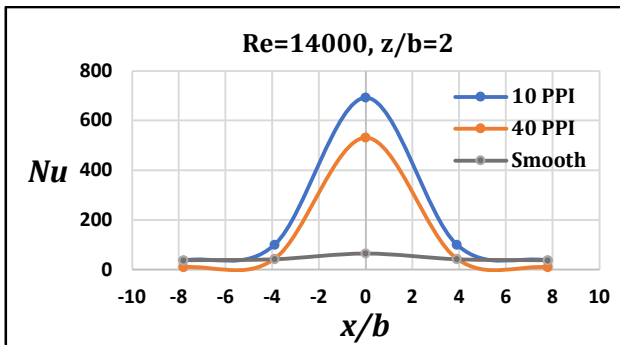
(a)



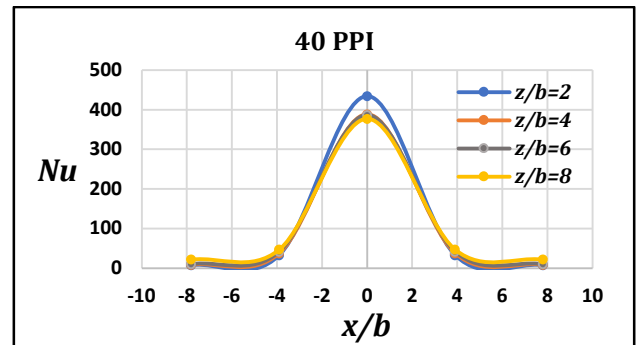
(b)



(b)



(c)



(c)

Figure 8: Variation of local Nusselt number on a smooth flat plate and copper foam flat plate for various Reynolds numbers at a slot-to-plate distance of 2.

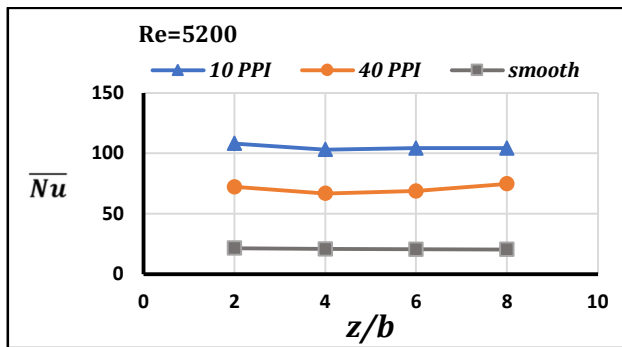
Figure 9: Influence of the distance between slot and plate on the local Nusselt number for copper foam flat plate and smooth flat plate at $Re=9600$.

4.3 Effect of slot-to-plate distance on local Nusselt number

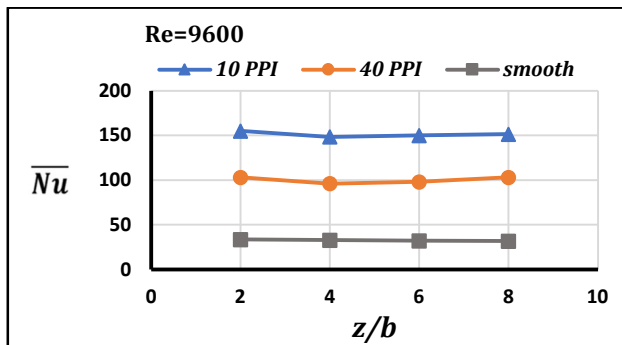
Figures (9a–c) illustrate the influence of an increment in slot-to-plate distance from 2 to 8 at Reynolds number 9600 on the local Nusselt numbers of (10 and 40 PPI) copper foam flat plate and smooth flat plate. According to Figure (9a), there was a small increase in the local Nusselt number of the smooth flat plate with each increment of the slot-to-plate distance. The local Nusselt number of the copper foam flat plate with a pore density of 10 and 40 PPI is found to be more significant, as Figures (9b–c) show. It is found that a peak higher local Nusselt number was achieved at a slot-to-plate distance of 2. For a slot-to-plate distance of 4, 6, and 8, the curve lines of the local Nusselt number overlapped. This increased slot-to-plate distance allowed more evenly distributed flow to penetrate the porous media.

4.4 The average Nusselt number (\overline{Nu})

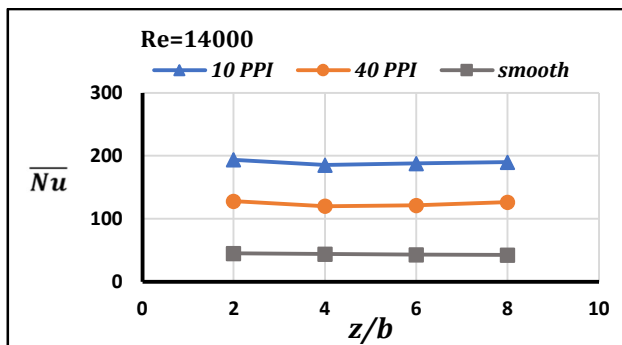
The variation of the average Nusselt numbers of copper foam flat plate and smooth flat plate with slot-to-plate distance for all the Reynolds numbers studied is seen in Figures (10a–c). For both a copper foam flat plate and a smooth flat plate, it has been found that average Nusselt numbers rise as Reynolds numbers increase. The average Nusselt number of a copper foam flat plate is higher than that of a smooth flat plate. At $Re=5200$ and $z/b=2$, results showed the average Nusselt number of a copper foam flat plate with 10 and 40 PPI enhanced by 73% and 72%, respectively compared to a smooth flat plate. A slot-to-plate distance had little effect on the average Nusselt numbers for all Reynolds numbers. However, the slot-to-plate distance of 2 impacted the average Nusselt numbers with all Reynolds numbers in this study.



(a)



(b)



(c)

Figure 10: Influence of the pore density on the average Nusselt numbers on the smooth flat plate and copper foam flat plate a) Re=5200, b) Re=9600, c) Re=14000.

5. Conclusion

The thermal characteristics of the copper foam flat plate and the smooth flat plate under the impinging jet were investigated experimentally. The effect of the density of pore of copper foam, slot-to-plate distance, and Reynolds number was investigated. The following is a summary of the study's highlights:

- Comparisons between the results of a copper foam flat plate and a smooth flat plate confirm that the copper foam structures enhance the local Nusselt number.
- The copper foam flat plate with a pore density of 10 PPI has a higher Nusselt number and heat

transfer rate compared to the copper flat plate with a pore density of 40 PPI.

- The current investigation has demonstrated that using copper foams significantly impacts the local and average Nusselt numbers.

Acknowledgments

The authors express gratitude to the Engineers in Heat Transfer Laboratory in the Department of Mechanical Engineering, College of Engineering, University of Baghdad, Iraqi Ministry of Higher Education and Scientific Research.

References

- [1] A. A. Karamallah, I. Y. Hussain, and D. H. Alwan, "Experimental Study of Natural Convection Heat Transfer in Confined Porous Media Heated From Side," *Journal of Engineering*, vol. 19, no. 8, pp. 952-969, 2013.
- [2] A. A. Mohammed, "Review on Heat Transfer Process Inside Open and Closed Porous Cavity," *Journal of Engineering*, vol. 26, pp. 204-216, 2020.
- [3] A. J. Onstad, C. J. Elkins, F. Medina, R. B. Wicker, J. K. Eaton, "Full-field measurements of flow through a scaled metal foam replica," *Exp Fluids*, vol. 50, pp. 1571-1585, 2011.
- [4] I. Y. Hussain and M. M. Saleh, "Natural convection in the confined cylindrical enclosure of porous media with constant and periodic wall temperature boundary conditions," *Journal of Engineering*, vol. 17, no. 2, pp. 347-365, 2011.
- [5] J. Issac, D. Singh, and S. Kango, "Experimental and numerical investigation of heat transfer characteristics of jet impingement on a flat plate," *Heat and Mass Transfer*, vol. 56, pp. 531-546, 2019.
- [6] J. Joshi and S. K. Sahu, "Heat transfer characteristics of flat and concave surfaces by circular and elliptical jet impingement," *Experimental Heat Transfer*, vol. 35, pp. 938-963, 2021.
- [7] J. P. Holman, "Experimental methods for engineers," Eight Ed. McGraw-Hill Series in Mechanical Engineering; 2007.
- [8] K. E. Amori and D. A. Khalaf, "Thermal analysis of metal foam heat sink subjected to impingement

- jet cooling, ” The Iraqi Journal For Mechanical And Material Engineering, vol. 15, pp. 12-30, 2015.
- [9] K. Yogi, S. Krishnan, S.V. Prabhu “Experimental investigation on the local heat transfer with an unconfined slot jet impinging on a metal foamed flat plate,” International Journal of Thermal Sciences, Vol. 169, 2021.
- [10]L. Dhruw, H. B. Kothadia, and A. Kumar R, “Experimental analysis of local and average heat transfer between circular impinging jet and flat plate,” Experimental Heat Transfer, vol. 36 pp. 1-25, 2022.
- [11]L. F. Ali, “Natural and Mixed Convection in Square Vented Enclosure Filled with Metal Foam,” Journal of Engineering, vol. 21, no. 11, pp. 60-79, 2015.
- [12]M. Nirmalkumar, V. Katti, and S.V. Prabhu, “Local heat transfer distribution on a smooth flat plate impinged by a slot jet,” International Journal of Heat and Mass Transfer, vol. 54, pp. 727–738, 2011.
- [13]P. K. Singh, J. Joshi, and S. K. Sahu, “Experimental Investigation to Identify the Effect of Thin Metal Foam on Heat Transfer Characteristics of a Heated Plate,” ISHMT-ASTFE, pp. 2541-2546, 2021.
- [14]R. M. K. Ali and S. L. Ghashim, “Numerical analysis of the heat transfer enhancement by using metal foam,” Case Studies in Thermal Engineering, vol 49, 2023.
- [15]R. M. K. Ali and S. L. Ghashim, “Thermal performance analysis of heat transfer in pipe by using metal foam,” Jordan Journal of Mechanical and Industrial Engineering, vol 17, No. 2, 2023.
- [16]R. Vinze, S. Chandel, M.D. Limaye, and S.V. Prabhu, “Influence of jet temperature and nozzle shape on the heat transfer distribution between a smooth plate and impinging air jets,” International Journal of Thermal Sciences, vol. 99, pp. 136-151, 2016.
- [17]R. Yakkatelli, Q. Wu, and A.S. Fleischer, “A visualization study of the flow dynamics of a single round jet impinging on porous media,” Experimental Thermal and Fluid Science, vol. 34, pp. 1008–1015, 2010.
- [18]S. N. Diop, B. Dieng, and I. Senaha, “A study on heat transfer characteristics by impinging jet with several velocities distribution,” Case Studies in Thermal Engineering, vol. 26, no. 2, 2021.
- [19]W. H. Shih, F. C. Chou, and W. H. Hsieh, “Experimental Investigation of the Heat Transfer Characteristics of Aluminum-Foam Heat Sinks With Restricted Flow Outlet,” Journal of Heat Transfer, vol. 129, no. 11, pp. 1554-1563, 2007.

Nomenclature

A	Surface area (m ²)
b	Width of the slot (m)
D_h	Hydraulic equivalent diameter (m)
h	Coefficient of convective heat transfer (W/m ² K)
I	Supplied current (A)
K_{air}	Air thermal conductivity (W/m K)
L_s	The slot length (m)
L	The length of the flat plate (m)
L_f	Length of foam (m)
ṁ	Mass flow rate (kg/s)
Nu	Local Nusselt number based on the width of the slot
Nū	Average Nusselt number based on the width of the slot
q_{joule}	Supplied heat flux, (W/m ²)
q_{loss}	Total heat flux loss from target surface (W/m ²)
q_{rad}	Radiation heat loss from the front surface of the impingement plate (W/m ²)
q_{nat}	Heat loss by natural convection from the back surface of the impingement plate (W/m ²)
Re	Reynolds number
T_{jet}	Air jet temperature (°C)
T_w	Surface temperature (°C)
T_{amb}	Ambient temperature (°C)
t_f	Foam thickness (m)
t_p	Thickness of the base plate (m)
V	Voltage (V)
v	Nozzle exit velocity (m/s)
W	Flat plate width (m)
W_f	Width of foam (m)
x	Stream wise distance (m)
x/b	non-dimensional stream wise distance
y	Span wise direction (m)
z	Slot-to-plate distance (m)
z/b	non-dimensional slot-to-plate distance

Greek symbols

μ	viscosity of air (Pa s)
ρ	density of air (kg/m ³)

دراسة الأداء الحراري لاصطدام الهواء النفثات على صفيحة مستوية من رغوة النحاس

ظفر فاضل علي¹ ، ساجدة لفته عشم^{2*}

¹قسم الهندسة الميكانيكية، كلية الهندسة، جامعة بغداد، بغداد، العراق، Dhafar.fadhel@gmail.com

²قسم الهندسة الميكانيكية، كلية الهندسة، جامعة بغداد، بغداد، العراق، Sajda_lafta@yahoo.com

الممثل: ظفر فاضل علي، Dhafar.fadhel@gmail.com

نشر في: 31 اذار 2025

الخلاصة – تم إجراء دراسة تجريبية للأداء الحراري لاصطدام النفث الصادر من فوهة واحدة مستطيلة الشكل على صفيحة مستوية ذات رغوة نحاسية. تم استخدام رغوة النحاس بسمك 10 ملم ومسامية 90%. تم إجراء التجارب على أعداد رينولدز المختلفة بمدى يتراوح من 5200 إلى 14000 وعلى مسافات مختلفة من الفوهة إلى الصفيحة امتد من 2 إلى 8. أظهرت النتائج أن التحسن الأكبر لعدد نسلت الموضوعي ظهر في الصفيحة المستوية ذات الرغوة النحاسية مقارنة بالصفيحة المستوية الملساء. تمت دراسة تأثير كثافة المسام على عدد نسلت الموضوعي والمتوسط للصفائح المستوية ذات الرغوة النحاسية ذات كثافة مسامية (10 PPI) و(40 PPI). يُظهر عدد نسلت الموضوعي والمتوسط للوحة المستوية الرغوية النحاسية بكثافة مسام (10 PPI) زيادة أعلى من الصفيحة المستوية ذات الرغوة النحاسية بكثافة مسام (40 PPI). تمت دراسة تأثير المسافة بين الفوهة والصفيحة على عدد نسلت الموضوعي والمتوسط. بالنسبة لحالة الصفيحة المستوية الملساء، يرتفع عدد نسلت الموضوعي قليلاً مع زيادة المسافة بين الفوهة والصفيحة. في حالة الصفيحة المستوية ذات الرغوة النحاسية، يتخلل التدفق بالتساوي المشتمت الحراري عندما تزداد المسافة بين الفوهة والصفيحة. يكون انحراف التدفق أكثر أهمية بالنسبة للرغوات المعدنية مع مسافة قليلة من الفوهة إلى الصفيحة وكثافة منخفضة للمسام. ومع ذلك، فإن الزيادة في عدد رينولدز تسمح للتدفق باختراق الوسائط المسامية بشكل أكثر توازناً.

الكلمات الرئيسية – " الاصطدام النفثات، كثافة مسام رغوة النحاس، نفث الفوهة غير المحجوز، عدد نسلت الموضوعي، رغوة النحاس " .